International Journal of Heat and Mass Transfer 73 (2014) 731–742

Contents lists available at ScienceDirect

International Journal of Heat and Mass Transfer

journal homepage: www.elsevier.com/locate/ijhmt

# Theoretical model for local heat transfer coefficient for annular flow boiling in circular mini/micro-channels

Sung-Min Kim, Issam Mudawar *

*Purdue University Boiling and Two-Phase Flow Laboratory (PU-BTPFL), Mechanical Engineering Building, 585 Purdue Mall, West Lafayette, IN 47907-2088, USA*

ARTICLE INFO

*Article history:*
Received 15 October 2013
Received in revised form 19 February 2014
Accepted 20 February 2014
Available online 19 March 2014

*Keywords:*
Evaporation
Annular flow
Eddy diffusivity
Mini-channel
Micro-channel

ABSTRACT

This study examines two-phase heat transfer characteristics associated with annular flow boiling in circular mini/micro-channels with circumferentially uniform heat flux. A theoretical control-volume-based model is developed based on the assumptions of smooth interface between the annular liquid film and vapor core, and uniform film thickness around the channel's circumference. Droplet entrainment and deposition effects are incorporated in the model with the aid of new correlations for initial liquid droplet quality at the onset of annular flow, and deposition mass transfer coefficient, respectively. The model also accounts for interfacial suppression of turbulent eddies due to surface tension with the aid of an eddy diffusivity model specifically tailored to shear-driven turbulent films. The model shows excellent predictive capability against 149 convective boiling dominant data points for saturated flow boiling in circular mini/micro-channels, evidenced by an overall mean absolute error of 16.5%, with 91.3% and 98.0% of the data falling within ±30% and ±50% error bands, respectively.



## 1. Introduction

Recent advances in applications such as high performance computers, electrical vehicle power electronics, avionics, and directed energy laser and microwave weapon systems have led to unprecedented challenges in removing large amounts of heat from very small areas [1–8]. While a variety of two-phase cooling schemes, including pool boiling [9–11], jet [12–15], spray [16–19], surface enhancement [20–22], and hybrid cooling techniques that combine the benefits of different schemes [23,24] have been considered for these applications, two-phase mini/micro-channel devices have been especially favored for their compactness, relative ease of fabrication, high heat dissipation to volume ratio, and small coolant inventory.

Studies on flow boiling in mini/micro-channels have resulted in different approaches to predicting pressure drop and heat transfer coefficient. The vast majority of these studies are based on Lockhart–Martinelli-type [25] separated flow models for pressure drop [26–30], and semi-empirical correlations for heat transfer coefficient [31–34]. However, these methods have been validated only for specific flow configurations and relatively narrow ranges of operating conditions. In pursuit of 'universal' predictive tools that are applicable to different working fluids and broad ranges of operating conditions, a series of studies have been conducted at the Purdue University Boiling and Two-Phase Flow Laboratory (PU-BTPFL), which involve systematic consolidation of world databases for mini/micro-channels, and development of universal predictive tools for pressure drop [35,36], heat transfer coefficient [37,38], and dryout incipience quality [39], following very closely a methodology that was adopted earlier to predict flow boiling critical heat flux (CHF) for water flow in tubes [40–42].

Another effective method to predicting pressure drop and heat transfer coefficient for annular two-phase flow in mini/micro-channels is the control-volume-based approach. Because annular flow consists of predominantly two separated phases – vapor core and annular liquid film – it lends itself better to theoretical modeling than dispersed flow regimes such as bubbly and slug flows. Fig. 1 shows a schematic of the convective boiling dominant regime that is associated with saturated inlet conditions and terminated with dryout. In a recent study by the authors [38,39], convective boiling was identified as one of two dominant heat transfer mechanisms for saturated flow boiling in mini/micro-channels. For this convective boiling dominant regime, bubbly and slug flow occupy a small portion of the channel length, while annular flow spans a significant fraction. Gradual evaporation and thinning of the annular liquid film cause the heat transfer coefficient to increase along the channel length. With a sufficiently high wall heat flux or sufficiently long channel, dryout of the

* Corresponding author. Tel.: +1 (765) 494 5705; fax: +1 (765) 494 0539.
*E-mail address:* mudawar@ecn.purdue.edu (I. Mudawar).
*URL:* https://engineering.purdue.edu/BTPFL (I. Mudawar).

http://dx.doi.org/10.1016/j.ijheatmasstransfer.2014.02.055
0017-9310/

**Nomenclature**

| | |
|---|---|
| $A$ | area |
| $A^+$ | constant in Eq. (47) |
| $A_{ch}$ | cross-sectional area of channel |
| $A_{f,*}$ | flow area of liquid control volume |
| $Bo$ | Boiling number, $q''_H/(Gh_{fg})$ |
| $C$ | liquid droplet concentration in vapor core |
| $Ca$ | Capillary number, $\mu_f G/(\rho_f \sigma)$ |
| $c_p$ | specific heat at constant pressure |
| $D$ | tube diameter |
| $D_h$ | hydraulic diameter |
| $D_{h,c}$ | hydraulic diameter of vapor core |
| $e$ | liquid droplet quality |
| $e_0$ | initial liquid droplet quality at onset of annular flow |
| $F$ | function |
| $f$ | Fanning friction factor; liquid film quality |
| $G$ | mass velocity |
| $h$ | heat transfer coefficient |
| $h_{fg}$ | latent heat of vaporization |
| $K$ | Von-Karman constant |
| $k$ | deposition mass transfer coefficient; thermal conductivity |
| $l^+$ | dimensionless turbulent mixing length |
| MAE | mean absolute error |
| $\dot{m}$ | mass flow rate |
| $P$ | pressure |
| $P_{crit}$ | critical pressure |
| $P_F$ | wetted perimeter |
| $P_{f,y}$ | local perimeter |
| $P_{f,\delta}$ | interfacial perimeter |
| $P_H$ | heated perimeter |
| $P_R$ | reduced pressure, $P/P_{crit}$ |
| $Pr$ | Prandtl number |
| $Pr_T$ | turbulent Prandtl number, $\varepsilon_m/\varepsilon_h$ |
| $q''$ | heat flux at distance $y$ from channel wall |
| $q''_H$ | heat flux based on heated perimeter of channel |
| $q''_w$ | uniform circumferential heat flux for circular tube |
| $Re$ | Reynolds number |
| $Re_c$ | effective Reynolds number of vapor core, $\rho_H(u_c - u_i)D_{h,c}/\mu_g$ |
| $Re_F$ | liquid film Reynolds number, $4\rho_f u_{f,m}\delta/\mu_f$ |
| $Re_f$ | superficial liquid Reynolds number, $G(1-x)D_h/\mu_f$ |
| $Re_{fo}$ | liquid-only Reynolds number, $GD_h/\mu_f$ |
| $Re_G$ | vapor core Reynolds number, $\rho_g u_c D_{h,c}/\mu_g$ |
| $T$ | temperature |
| $T^+$ | dimensionless temperature |
| $u$ | velocity |
| $u^+$ | dimensionless velocity |
| $u^*$ | friction velocity |
| $u_{f,m}$ | mean liquid film velocity |
| $v$ | specific volume |
| $W$ | deposition rate |
| $We$ | Weber number, $G^2D_h/(\rho_f \sigma)$ |
| $x$ | vapor quality |
| $x_0$ | vapor quality at onset of annular flow |
| $x_c$ | effective vapor quality in vapor core |
| $x_e$ | thermodynamic equilibrium quality |
| $X_{tt}$ | Lockhart–Martinelli parameter based on turbulent liquid-turbulent vapor flows |
| $y$ | distance perpendicular to channel wall |
| $y^+$ | dimensionless distance perpendicular to channel wall, $yu^*/\nu_f$ |
| $z$ | stream-wise distance |

*Greek symbols*

| | |
|---|---|
| $\Gamma_d$ | deposition mass transfer rate per unit channel length |
| $\Gamma_{fg}$ | evaporation mass transfer rate per unit channel length |
| $\delta$ | thickness of annular liquid film |
| $\delta^+$ | dimensionless thickness, $\delta u^*/\nu_f$ |
| $\varepsilon_h$ | eddy heat diffusivity |
| $\varepsilon_m$ | eddy momentum diffusivity |
| $\mu$ | dynamic viscosity |
| $\nu$ | kinematic viscosity |
| $\rho$ | density |
| $\rho_H$ | homogeneous density of vapor core |
| $\sigma$ | surface tension |
| $\tau$ | shear stress |

*Subscripts*

| | |
|---|---|
| *avg* | average |
| *c* | vapor core |
| *cb* | convective boiling dominant heat transfer |
| *e* | entrained liquid |
| *exp* | experimental (measured) |
| *f* | saturated liquid; liquid film |
| *fo* | liquid only |
| *g* | saturated vapor |
| *i* | interfacial |
| *nb* | nucleate boiling dominant heat transfer |
| *pred* | predicted |
| *sat* | saturation |
| *tp* | two-phase |
| *w* | wall |

annular film ensues at a location downstream where the heat transfer coefficient begins to decrease appreciably.

The control-volume-based approach proved effective in predicting a variety of two-phase flow configurations, including pool boiling [10,11], separated flow boiling [43–48], and flow boiling in micro-channel heat sinks [49]. Recently, the authors of the present study also used this approach to construct a new model for annular condensation in mini/micro-channel flows [50].

Nonetheless, several fundamental challenges remain when attempting to develop an accurate model for annular flow boiling. These include interfacial instabilities, interfacial mass, momentum and heat transfer, and turbulence within the annular film. Two other sources of difficulty are droplet entrainment and droplet deposition. Entrainment refers to tiny liquid droplets breaking off the crests of waves and driven along with the vapor core. Deposition refers to droplets from the vapor core falling back upon the film interface. As indicated by Qu and Mudawar [51], the annular regime in flow boiling is initiated far upstream in a micro-channel, with an abundance of entrained droplets that are formed mostly by shattering of liquid from the micro-channel's upstream bubbly and slug flows.

The primary goal of the present study is to develop a theoretical control-volume-based model for annular flow boiling in mini/micro-channels. To assess the accuracy of the model, convective boiling dominant heat transfer data for saturated flow boiling in circular mini/micro-channels are compiled from six sources [52–57] as indicated in Table 1. Since two heat transfer regimes exist for flow boiling in mini/micro-channels, nucleate boiling dominant

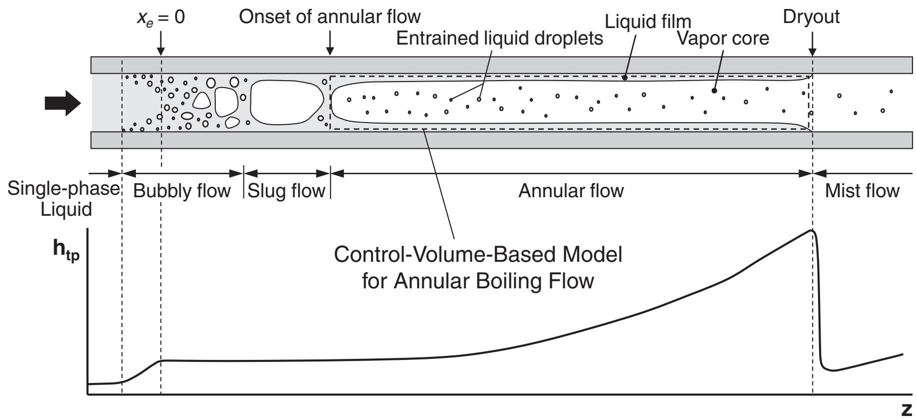


**Fig. 1.** Schematics of flow regimes, and variation of heat transfer coefficient along uniformly heated mini/micro-channel for convective boiling dominant heat transfer.

**Table 1**
Convective boiling dominant heat transfer data for saturated flow boiling in circular mini/micro-channels with corresponding mean absolute error (MAE) values for predictions of present model.

| Author(s) | Fluid(s) | $D$ [mm] | $G$ [kg/m$^2$s] | $q''_w$ [W/cm$^2$] | $x$ | $x_0$[a] | $(h_{nb}/h_{cb})_{avg}$[b] | Number of data points | MAE [%] |
|---|---|---|---|---|---|---|---|---|---|
| Sumith et al. [52] | Water | 1.45 | 106.5 | 20.9 | 0.02–0.22 | 0.01 | 0.29 | 5 | 30.5 |
| | | 1.45 | 152.7 | 20.9 | 0.02–0.15 | 0.01 | 0.33 | 5 | 22.8 |
| Saitoh et al. [53] | R134a | 1.12 | 300 | 1.3 | 0.21–0.83 | 0.08 | 0.56 | 35 | 15.0 |
| | | 3.1 | 300 | 1.2 | 0.21–0.84 | 0.07 | 0.57 | 26 | 15.2 |
| Ohta et al. (2009) [54] | FC72 | 0.51 | 107 | 0.9 | 0.07–0.70 | 0.06 | 0.79 | 10 | 12.5 |
| Bang et al. [55] | Water | 1.73 | 100 | 5.0 | 0.02–0.56 | 0.02 | 0.14 | 12 | 26.1 |
| | | 1.73 | 100 | 8.0 | 0.04–0.45 | 0.02 | 0.19 | 10 | 8.1 |
| | | 1.73 | 100 | 11.5 | 0.06–0.45 | 0.02 | 0.24 | 10 | 14.1 |
| Oh and Son [56] | R22 | 1.77 | 400 | 1.0 | 0.12–0.96 | 0.08 | 0.53 | 7 | 31.6 |
| Li et al. [57] | R32 | 2.0 | 202 | 0.6 | 0.36–0.80 | 0.11 | 0.41 | 29 | 13.3 |
| Total | | | | | | | | 149 | 16.5 |

[a] Vapor quality at location of the onset of annular flow, which is determined according to Taitel and Dukler [59] ($X_{tt}$ = 1.6).
[b] Average value of $h_{nb}/h_{cb}$ for individual database, where $h_{nb}$ and $h_{cb}$ are calculated using Table 2.

and convective boiling dominant, only the convective boiling dominant data associated with annular film evaporation are used. The selected data are obtained from the original database amassed by Kim and Mudawar [38]. In addition, only local heat transfer coefficient data are considered; data averaged over the channel length are excluded. The database that is compared to the model predictions consists of 149 heat transfer data points covering five different working fluids, water, FC72, R134a, R22 and R32, hydraulic diameters from 0.51 to 3.1 mm, mass velocities from 100 to 400 kg/m$^2$s, wall heat fluxes from 0.6 to 20.9 W/cm$^2$, and qualities from 0.02 to 0.96. To achieve closure in the new model development, correlations are developed for initial liquid droplet quality at the onset of annular flow and the deposition mass transfer coefficient.

## 2. Model development

### 2.1. Model assumptions

Fig. 2 provides a schematic representation of liquid film evaporation in a circular channel with a circumferentially uniform heat flux. Annular flow consists of a thin liquid film that travels along the channel wall, a continuous vapor core along the center of the channel, and liquid droplets entrained in the vapor core. Following are key assumptions of the model.

(1) The annular flow is steady, incompressible, and concurrent.
(2) Pressure is uniform across the channel's cross-sectional area.
(3) Thermodynamic equilibrium is maintained along the channel.

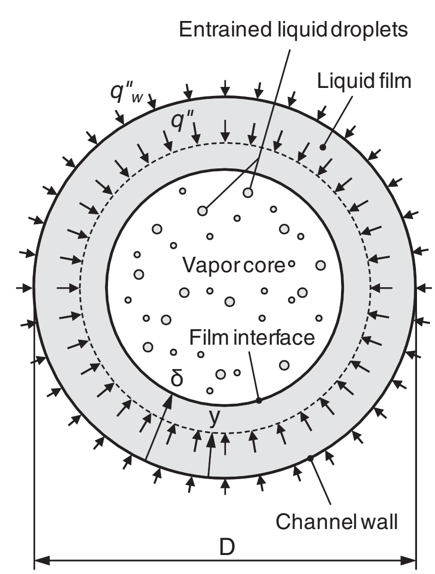


**Fig. 2.** Schematic of liquid film evaporation in mini/micro-channel with uniform circumferential heat flux.

(4) Gravitational effects are negligible due to high shear stresses in mini/micro-channels.
(5) The liquid film interface is smooth, and liquid film thickness is circumferentially uniform due to strong surface tension effects in mini/micro-channels.

(6) Axial momentum changes in the liquid film are negligible due to the relatively small velocity of the liquid film.
(7) Mass transfer occurs only at the vapor–liquid interface.
(8) Heat flux is uniform along the vapor–liquid interface.
(9) Entrainment of liquid droplets occurs entirely by shattering of liquid from collapse of upstream bubbly/slug flow regimes.
(10) Deposition rate of entrained liquid droplets is circumferentially uniform.

### 2.2. Control volume analysis

The total mass flow rate, $\dot{m}$, in the flow channel can be expressed as

$$\dot{m} = \dot{m}_f + \dot{m}_e + \dot{m}_g, \tag{1}$$

where $\dot{m}_f$, $\dot{m}_e$, and $\dot{m}_g$ are the mass flow rates of the liquid film, entrained liquid droplets and vapor core, respectively, and their ratios to the total mass flow rate are defined as the liquid film quality, $f$, liquid droplet quality, $e$, and vapor quality, $x$, respectively,

$$f = \frac{\dot{m}_f}{\dot{m}}, \tag{2}$$

$$e = \frac{\dot{m}_e}{\dot{m}}, \tag{3}$$

and

$$x = \frac{\dot{m}_g}{\dot{m}}. \tag{4}$$

Based on assumption (4), the vapor quality is set equal to the thermodynamic equilibrium quality,

$$x = x_e. \tag{5}$$

Qu and Mudawar [58] used Taitel and Dukler's [59] flow regime map to determine the boundary between intermittent and annular flow in their analytical model for laminar micro-channel flow with $X_{vv}$ = 1.6. In the present study, the original formulation of the Taitel and Dukler map, which is based on Lockhart–Martinelli's parameter for the combination of turbulent liquid and turbulent vapor flow [25] is used to determine this boundary,

$$X_{tt} = \left(\frac{\mu_f}{\mu_g}\right)^{0.1}\left(\frac{1-x}{x}\right)^{0.9}\left(\frac{\rho_g}{\rho_f}\right)^{0.5} = 1.6. \tag{6}$$

Rearranging Eq. (6) yields the following relation for initial vapor quality at the onset of annular flow,

$$x_0 = \left[1 + 1.6^{1/0.9}\left(\frac{\mu_f}{\mu_g}\right)^{-1/9}\left(\frac{\rho_g}{\rho_f}\right)^{-1/1.8}\right]^{-1}. \tag{7}$$

As indicated in Table 1, all initial vapor quality values of individual databases predicted by Eq. (7) are smaller than the experimental quality ranges. This confirms that all the convective boiling dominant data in Table 1 fall into the annular flow regime.

For the prediction of initial liquid entrainment quality of water flow boiling in micro-channels, Qu and Mudawar [58] modified a value proposed earlier by Whalley et al. [60] to account for the effects of mass velocity and surface tension using the Weber number.

$$We_{fo} = \frac{G^2 D_h}{\rho_f \sigma}. \tag{8}$$

A new correlation is developed for initial liquid droplet quality at the onset of annular flow, which yields least MAE values between the model predictions and the experimental mini/micro-channel data summarized in Table 1,

$$e_0 = 0.951 - 0.32 Ca^{0.21} P_R^{-0.42}, \tag{9}$$

where the Capillary number and reduced pressure, which are used to cope with both different working fluids and broad ranges of operating conditions, are defined, respectively, as

$$Ca = \frac{\mu_f G}{\rho_f \sigma} = \frac{We_{fo}}{Re_{fo}} \tag{10}$$

and

$$P_R = \frac{P}{P_{crit}}. \tag{11}$$

To develop a theoretical control-volume-based model, mass and momentum conservation are first applied to control volumes encompassing the liquid film and vapor core separately. Mass conservation for the liquid film, entrained liquid droplets, and vapor core are expressed, respectively, as

$$\frac{d\dot{m}_f}{dz} + \Gamma_{fg} - \Gamma_d = 0, \tag{12}$$

$$\frac{d\dot{m}_e}{dz} + \Gamma_d = 0 \tag{13}$$

and

$$\frac{d\dot{m}_g}{dz} - \Gamma_{fg} = 0. \tag{14}$$

The mass flow rate of the liquid film, and rates of mass transfer due to evaporation and deposition can be expressed, respectively, as

$$\dot{m}_f = \rho_f \int_0^\delta u_f P_{f,y}\, dy, \tag{15}$$

$$\Gamma_{fg} = \frac{q''_w P_H}{h_{fg}} \tag{16}$$

and

$$\Gamma_d = W P_{f,\delta}, \tag{17}$$

where the local perimeter, $P_{f,y}$, heated perimeter, $P_H$, and interfacial perimeter, $P_{f,\delta}$, are expressed, respectively, as

$$P_{f,y} = \pi(D - 2y), \tag{18}$$

$$P_H = \pi D \tag{19}$$

and

$$P_{f,\delta} = \pi(D - 2\delta). \tag{20}$$

As discussed by Qu and Mudawar [58], droplet deposition from the vapor core to the annular liquid film is a highly complex phenomenon, which explains why researchers have relied on empirical methods to evaluate its influence on the heat transfer coefficient. According to Whalley et al. [60] and Paleev and Filippovich [61], droplet deposition is assumed a mass transfer process yielding a linear relationship between deposition rate, $W$, and liquid droplet concentration, $C$, in the vapor core,

$$W = kC, \tag{21}$$

where $C$ is defined as

$$C = \frac{\dot{m}_e}{\dot{m}_g v_g + \dot{m}_e v_f}, \tag{22}$$

**Table 2**
Kim and Mudawar's [38,39] correlation for pre-dryout saturated flow boiling heat transfer in mini/micro-channels.

$$h_{tp} = \left(h_{nb}^2 + h_{cb}^2\right)^{0.5}$$

$$h_{nb} = \left[2345\left(Bo\frac{P_H}{P_F}\right)^{0.70} P_R^{0.38}(1-x)^{-0.51}\right]\left(0.023\,Re_f^{0.8}Pr_f^{0.4}\frac{k_f}{D_h}\right)$$

$$h_{cb} = \left[5.2\left(Bo\frac{P_H}{P_F}\right)^{0.08} We_{fo}^{-0.54} + 3.5\left(\frac{1}{X_{tt}}\right)^{0.94}\left(\frac{\rho_g}{\rho_f}\right)^{0.25}\right]\left(0.023\,Re_f^{0.8}\,Pr_f^{0.4}\frac{k_f}{D_h}\right)$$

where $Bo = \frac{q''_H}{G h_{fg}}, P_R = \frac{P}{P_{crit}}, Re_f = \frac{G(1-x)D_h}{\mu_f}, We_{fo} = \frac{G^2 D_h}{\rho_f \sigma}, X_{tt} = \left(\frac{\mu_f}{\mu_g}\right)^{0.1}\left(\frac{1-x}{x}\right)^{0.9}\left(\frac{\rho_g}{\rho_f}\right)^{0.5}$

$q''_H$ is effective heat flux averaged over heated perimeter of channel, $P_H$ is heated perimeter of channel, $P_F$ is wetted perimeter of channel

For a circular tube with uniform circumferential heat flux $q''_w, q''_H = q''_w$ and $\frac{P_H}{P_F} = 1$

and $k$ is the deposition mass transfer coefficient, which has the units of velocity. Qu and Mudawar [58], Hewitt and Govan [62] and Sugawara [63] proposed different correlations for $k$ based on the popular functional form of Paleev and Filippovich [61]. In the present study, the Paleev and Filippovich correlation is modified by introducing both density ratio and reduced pressure to tackle different working fluids and broad ranges of operating conditions. The following correlation for $k$ is proposed, which yields the least MAE values between the model predictions and the experimental mini/micro-channel data summarized in Table 1,

$$\frac{k}{u_c} = 0.0018\left(\frac{\rho_g u_c D}{\mu_g}\right)^{-0.26}\left(\frac{C}{\rho_g}\right)^{-0.28}\left(\frac{\rho_g}{\rho_f}\right)^{0.63} P_R^{-1.57}, \tag{23}$$

where $u_c$, $A_c$, $\rho_H$ and $x_c$ are, respectively, the mean velocity, flow area, homogeneous density, and effective vapor quality of the vapor core, which are defined as

$$u_c = \frac{\dot{m}_g + \dot{m}_e}{\rho_H A_c}, \tag{24}$$

$$A_c = \frac{\pi}{4}(D - 2\delta)^2, \tag{25}$$

$$\rho_H = \frac{1}{x_c v_g + (1 - x_c) v_f}, \tag{26}$$

and

$$x_c = \frac{\dot{m}_g}{\dot{m}_g + \dot{m}_e}. \tag{27}$$

Applying momentum conservation to the liquid film control volume depicted in Fig. 3(a) yields

$$\Gamma_{fg} u_i \Delta z - \Gamma_d u_c \Delta z = P A_{f,*} - \left(P + \frac{dP}{dz}\Delta z\right) A_{f,*} - \tau P_{f,y}\Delta z + \tau_i P_{f,\delta}\Delta z, \tag{28}$$

where the flow area, $A_{f,*}$, is expressed as

$$A_{f,*} = \frac{\pi}{4}(D - 2y)^2 - \frac{\pi}{4}(D - 2\delta)^2. \tag{29}$$

Rearranging Eq. (28) gives

$$\tau = \left(-\frac{dP}{dz}\right)\frac{A_{f,*}}{P_{f,y}} + \frac{\tau_i P_{f,\delta} + \Gamma_d u_c - \Gamma_{fg} u_i}{P_{f,y}}. \tag{30}$$

Allowing for turbulence in the liquid film, the local shear stress in the film can be expressed as

$$\tau = \mu_f\left(1 + \frac{\varepsilon_m}{\nu_f}\right)\frac{du_f}{dy}, \tag{31}$$

where $\varepsilon_m$ is the eddy momentum diffusivity. Substituting Eq. (31) into Eq. (30) and integrating yield the velocity profile across the liquid film,

$$u_f(y) = \frac{\delta}{\mu_f}\left(-\frac{dP}{dz}\right)\int_0^{y/\delta}\frac{A_{f,*}}{P_{f,y}}\left(1 + \frac{\varepsilon_m}{\nu_f}\right)^{-1} d\left(\frac{y}{\delta}\right) + \frac{\delta}{\mu_f}\left(\tau_i P_{f,\delta} + \Gamma_d u_c - \Gamma_{fg} u_i\right)\int_0^{y/\delta}\frac{1}{P_{f,y}}\left(1 + \frac{\varepsilon_m}{\nu_f}\right)^{-1} d\left(\frac{y}{\delta}\right). \tag{32}$$

The interfacial velocity can be determined by setting $y = \delta$ in Eq. (32),

$$u_i = \frac{\left(-\frac{dP}{dz}\right)\int_0^1 \frac{A_{f,*}}{P_{f,y}}\left(1 + \frac{\varepsilon_m}{\nu_f}\right)^{-1} d\left(\frac{y}{\delta}\right) + \left(\tau_i P_{f,\delta} + \Gamma_d u_c\right)\int_0^1 \frac{1}{P_{f,y}}\left(1 + \frac{\varepsilon_m}{\nu_f}\right)^{-1} d\left(\frac{y}{\delta}\right)}{\frac{\mu_f}{\delta} + \Gamma_{fg}\int_0^1 \frac{1}{P_{f,y}}\left(1 + \frac{\varepsilon_m}{\nu_f}\right)^{-1} d\left(\frac{y}{\delta}\right)}. \tag{33}$$

Substituting Eq. (32) into Eq. (15) yields the following relation for pressure gradient,

$$-\frac{dP}{dz} = \frac{\frac{\mu_f \dot{m}_f}{\rho_f \delta^2} - \left(\tau_i P_{f,\delta} + \Gamma_d u_c - \Gamma_{fg} u_i\right)\int_0^1\left[P_{f,y}\int_0^{y/\delta}\frac{1}{P_{f,y}}\left(1 + \frac{\varepsilon_m}{\nu_f}\right)^{-1} d\left(\frac{y}{\delta}\right)\right] d\left(\frac{y}{\delta}\right)}{\int_0^1\left[P_{f,y}\int_0^{y/\delta}\frac{A_{f,*}}{P_{f,y}}\left(1 + \frac{\varepsilon_m}{\nu_f}\right)^{-1} d\left(\frac{y}{\delta}\right)\right] d\left(\frac{y}{\delta}\right)}. \tag{34}$$

The double integral terms in the above equation can be expanded as

$$\int_0^1\left[P_{f,y}\int_0^{y/\delta} F(y)\, d\left(\frac{y}{\delta}\right)\right] d\left(\frac{y}{\delta}\right) = \pi D\int_0^1\left[\int_0^{y/\delta} F(y)\, d\left(\frac{y}{\delta}\right)\right] d\left(\frac{y}{\delta}\right) + \pi\delta\int_0^1\left[\left(\frac{y}{\delta}\right)^2 - 1\right] F(y)\, d\left(\frac{y}{\delta}\right). \tag{35}$$

Applying momentum conservation to the vapor core control volume depicted in Fig. 3(b) yields

$$\rho_H u_c^2 A_c + \frac{d\left(\rho_H u_c^2 A_c\right)}{dz}\Delta z - \rho_H u_c^2 A_c + \Gamma_d u_c \Delta z - \Gamma_{fg} u_i \Delta z = P A_c - \left[P A_c + \frac{d(P A_c)}{dz}\Delta z\right] - \tau_i P_{f,\delta}\,\Delta z + \left(P + \frac{1}{2}\frac{dP}{dz}\Delta z\right)\frac{dA_c}{dz}\Delta z. \tag{36}$$

Rearranging Eq. (36) and neglecting the second order term of $\Delta z$ yield the following relation for interfacial shear stress between the liquid film and vapor core,

$$\tau_i = \frac{1}{P_{f,\delta}}\left[A_c\left(-\frac{dP}{dz}\right) - \frac{d\left(\rho_H u_c^2 A_c\right)}{dz} - \Gamma_d u_c + \Gamma_{fg} u_i\right]. \tag{37}$$

The interfacial shear stress is the result of velocity differences between the vapor core and interface, modified by the influence of interfacial momentum transfer along the vapor–liquid interface due to evaporation; the later is based on a treatment by Wallis [64],

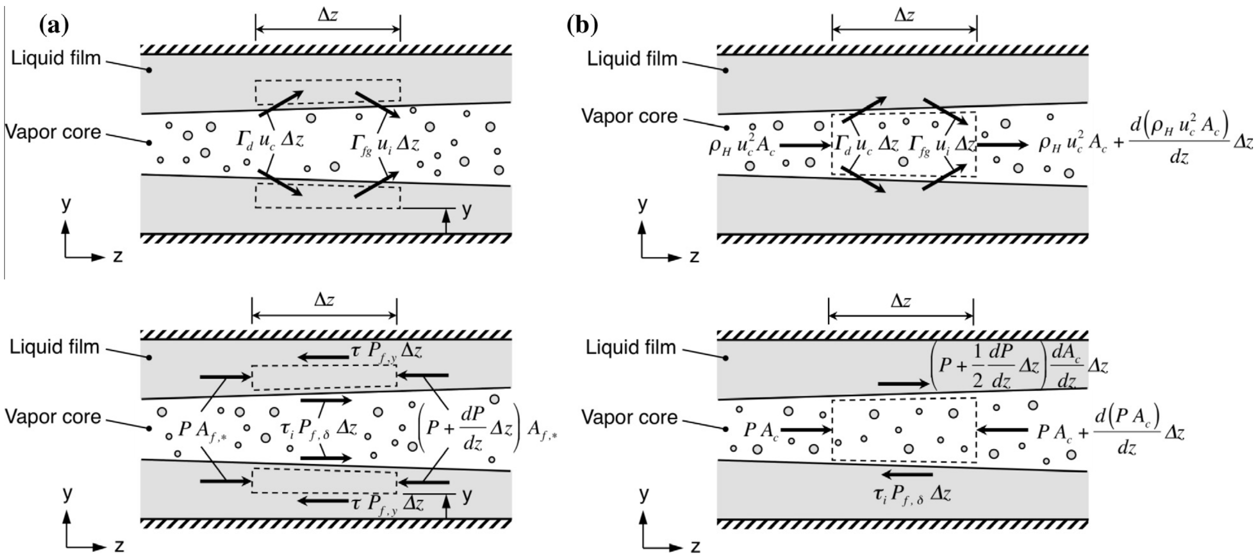


**Fig. 3.** Momentum and force components for (a) liquid film control volume and (b) vapor core control volume.

$$\tau_i = \frac{1}{2} f_i \rho_H (u_c - u_i)^2 - \frac{(u_c - u_i)\Gamma_{fg}}{2P_{f,\delta}}. \tag{38}$$

The interfacial friction factor, $f_i$, can be determined from relations by Shah and London [65],

$$f_i = 16\,Re_c^{-1} \text{ for } Re_c < 2000, \tag{39a}$$

$$f_i = 0.079\,Re_c^{-0.25} \text{ for } 2000 \leqslant Re_c < 20{,}000 \tag{39b}$$

and

$$f_i = 0.046\,Re_c^{-0.2} \text{ for } Re_c \geqslant 20{,}000, \tag{39c}$$

where $Re_c$ and $D_{h,c}$ are the effective Reynolds number and hydraulic diameter of the vapor core, respectively, which are given by

$$Re_c = \frac{\rho_H (u_c - u_i) D_{h,c}}{\mu_g} \tag{40}$$

and

$$D_{h,c} = \frac{4A_c}{P_{f,\delta}}. \tag{41}$$

### 2.3. Turbulence model

Eq. (31) can be expressed in nondimensional form as

$$\frac{\tau}{\tau_w} = \left(1 + \frac{\varepsilon_m}{\nu_f}\right)\frac{du^+}{dy^+}, \tag{42}$$

where

$$u^+ = \frac{u}{u^*}, \tag{43}$$

$$y^+ = \frac{y u^*}{\nu_f} \tag{44}$$

and

$$u^* = \left(\frac{\tau_w}{\rho_f}\right)^{0.5}. \tag{45}$$

Based on the Prandtl mixing length theory, the eddy diffusivity can be expressed in terms of the turbulent mixing length according to the relation

$$\frac{\varepsilon_m}{\nu_f} = l^{+2}\frac{du^+}{dy^+}. \tag{46}$$

A turbulent mixing length relation originally proposed by Van Driest [66] was modified by Kays [67,68] to

$$l^+ = Ky^+\left[1 - exp\left(-\sqrt{\frac{\tau}{\tau_w}}\frac{y^+}{A^+}\right)\right], \tag{47}$$

where $K = 0.4$ is the Von-Karman constant and $A^+$ is given by [67,68]

$$A^+ = 26\left(1 + 30.18\,\mu_f \rho_f^{-0.5} \tau_w^{-1.5}\frac{dP}{dz}\right)^{-1}. \tag{48}$$

Substituting Eqs. (42) and (47) into Eq. (46) yields the following eddy diffusivity profile,

$$\frac{\varepsilon_m}{\nu_f} = -\frac{1}{2} + \frac{1}{2}\sqrt{1 + 4K^2 y^{+2}\left[1 - exp\left(-\sqrt{\frac{\tau}{\tau_w}}\frac{y^+}{A^+}\right)\right]^2 \frac{\tau}{\tau_w}}. \tag{49}$$

To account for interfacial dampening in the liquid film due to suppression of turbulent eddies by surface tension, a dampening term, $(1 - y^+/\delta^+)^{0.1}$, is included in the above eddy diffusivity profile [50]. The complete form of eddy momentum diffusivity in the shear-driven film is expressed as

$$\frac{\varepsilon_m}{\nu_f} = -\frac{1}{2} + \frac{1}{2} \times \sqrt{1 + 4K^2 y^{+2}\left[1 - exp\left(-\sqrt{\frac{\tau}{\tau_w}}\frac{y^+}{A^+}\right)\right]^2 \frac{\tau}{\tau_w}\left(1 - \frac{y^+}{\delta^+}\right)^{0.1}}, \tag{50}$$

where, based on Eq. (30),

$$\frac{\tau}{\tau_w} = \frac{\pi D}{P_{f,y}} \frac{\left(-\frac{dP}{dz}\right)A_{f,*} + \tau_i P_{f,\delta} + \Gamma_d u_c - \Gamma_{fg} u_i}{\left(-\frac{dP}{dz}\right)\pi\delta(D - \delta) + \tau_i P_{f,\delta} + \Gamma_d u_c - \Gamma_{fg} u_i}. \tag{51}$$

### 2.4. Determination of heat transfer coefficient

Heat flux across the liquid film is related to the liquid temperature gradient by the relation

$$\frac{q''}{q''_w} = \left(\frac{1}{Pr_f} + \frac{1}{Pr_T}\frac{\varepsilon_m}{\nu_f}\right)\frac{dT^+}{dy^+}, \tag{52}$$

where $T^+$ is the dimensionless temperature defined as

$$T^+ = \frac{\rho_f c_{p,f} u^* (T - T_w)}{q''_w} \tag{53}$$

and $Pr_T$ is the turbulent Prandtl number ($\varepsilon_m/\varepsilon_h$), which, as discussed by Mudawar and El-Masri [69], can be evaluated from the experimental data of Ueda et al. [70],

$$Pr_T = 1.4 \exp\left(-15\frac{y^+}{\delta^+}\right) + 0.66. \tag{54}$$

Integrating Eq. (52), the dimensionless temperature profile across the liquid film can be expressed as

$$T^+ = \int_0^{y^+} \frac{q''}{q''_w}\left(\frac{1}{Pr_f} + \frac{1}{Pr_T}\frac{\varepsilon_m}{\nu_f}\right)^{-1} dy^+, \tag{55}$$

where

$$\frac{q''}{q''_w} = \frac{P_H}{P_{f,y}} = \frac{D}{D - 2y}. \tag{56}$$

Therefore, the local boiling heat transfer coefficient can be expressed as

$$h_{tp} = \frac{q''_w}{T_{sat} - T_w} = \frac{\rho_f c_{p,f} u^*}{T^+_\delta} = \frac{\rho_f c_{p,f} u^*}{\int_0^{\delta^+} \frac{q''}{q''_w}\left(\frac{1}{Pr_f} + \frac{1}{Pr_T}\frac{\varepsilon_m}{\nu_f}\right)^{-1} dy^+}. \tag{57}$$

### 2.5. Calculation procedure

The model equations are solved numerically using a finite difference technique. The axial distance is divided into small $\Delta z$ increments and calculations are repeated staring at the upstream location corresponding to the onset of annular flow. The calculation procedure is as follows:

(1) The initial vapor quality, $x_0$, and initial liquid droplet quality, $e_0$, at the onset of annular flow are calculated using Eqs. (7) and (9), respectively. $\varepsilon_m/\nu_f$, $\delta$ and $-dP/dz$ are initialized to zero at the location of the onset of annular flow.
(2) $\varepsilon_m/\nu_f$ at the next $\Delta z$ location is calculated using Eq. (50) and values of the wall shear stress, $\tau_w$, interfacial shear, $\tau_i$, interfacial velocity, $u_i$, and pressure gradient, $-dP/dz$, at the node immediately upstream.
(3) An initial value of the film thickness $\delta$ is assumed, which is sufficiently smaller than $\delta$ at the node immediately upstream.
(4) The interfacial velocity, $u_i$, interfacial friction factor, $f_i$, interfacial shear, $\tau_i$, and pressure gradient, $-dP/dz$, are calculated using Eqs. (33), (39a), (39b), (39c), (38), and (34), respectively.
(5) Convergence is checked by comparing the two sides of Eq. (37). If the sides are not equal, $\varepsilon_m/\nu_f$ is updated with new values of $\tau_w$, $\tau_i$, $u_i$, and $-dP/dz$ at the present node, and steps (3)–(5) are repeated with a small $\Delta\delta$ increment until the correct value for $\delta$ is found.
(6) $\varepsilon_m/\nu_f$ is calculated using Eq. (50) and steps (2)–(6) repeated for the next downstream node. The values of $\delta$ and $-dP/dz$ at the next downstream node are then utilized as input for the previous upstream node. Steps (2)–(6) are repeated until the value of $\delta$ converges at the location of the onset of annular flow.

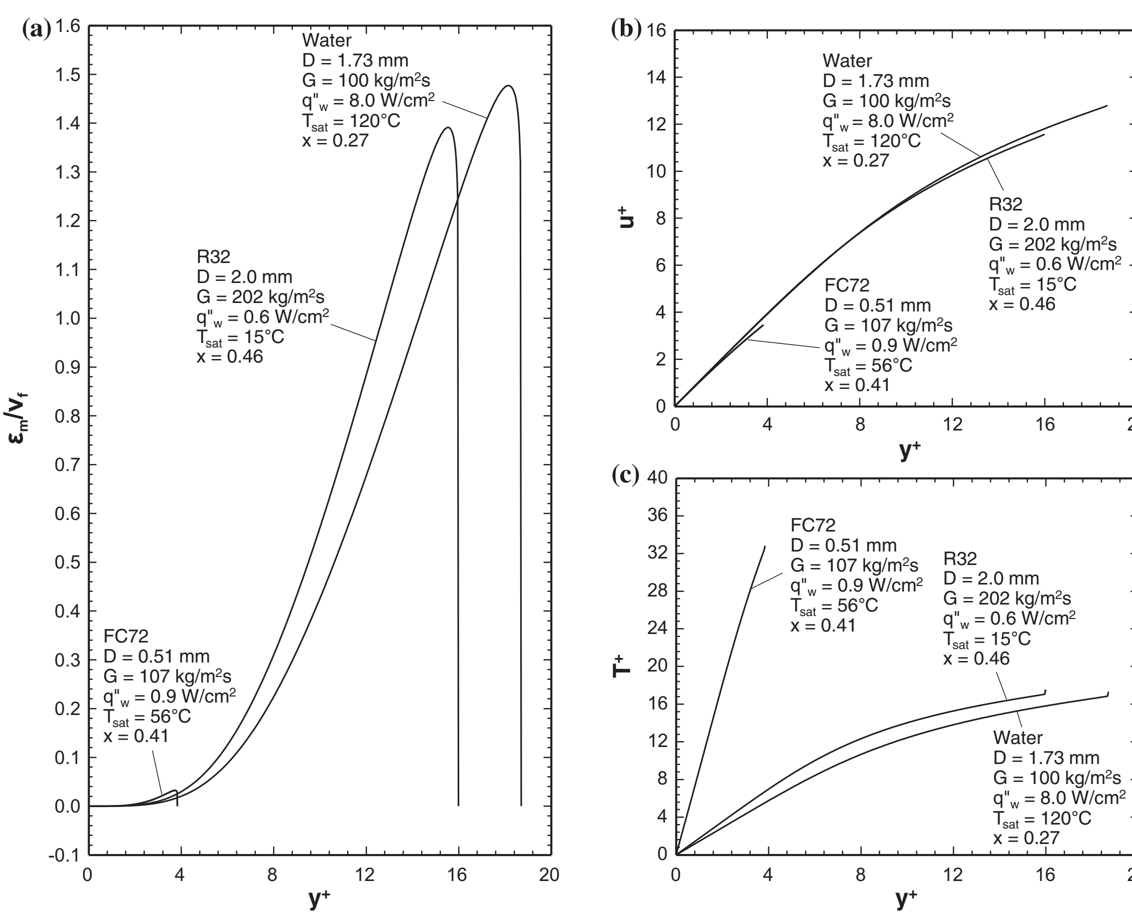


**Fig. 4.** (a) Eddy momentum diffusivity, (b) velocity, and (c) temperature profiles across evaporating liquid film in middle of channel for FC72, water, and R32 corresponding to operating conditions of Ohta et al. [54], Bang et al. [55] and Li et al. [57], respectively.

(7) The values of $\varepsilon_m/\nu_f$, $u^+$, $T^+$, and $h_{tp}$ are calculated using Eqs. (50), (43), (55), and (57), respectively. Steps (2)–(5) and (7) are then repeated for the next downstream node. The calculation procedure is continued until the last node is reached.

### 2.6. Simplified model

Since the thickness of the liquid film is generally small compared to the channel diameter, a simplified model is also derived using the following assumption,

$$P_{f,y} = P_{f,\delta} = P_f = \pi D. \tag{58}$$

Therefore, the flow area and mass flow rate of the liquid film can be expressed, respectively, as

$$A_{f,*} = P_f(\delta - y) \tag{59}$$

and

$$\dot{m}_f = \rho_f P_f \int_0^\delta u_f dy. \tag{60}$$

Applying momentum conservation to an annular element of the liquid film yields the following relation for shear stress,

$$\frac{\tau}{\tau_w} = \frac{-\frac{dP}{dz}(\delta - y) + \tau_i + \frac{\Gamma_d u_c - \Gamma_{fg} u_i}{\pi D}}{-\frac{dP}{dz}\delta + \tau_i + \frac{\Gamma_d u_c - \Gamma_{fg} u_i}{\pi D}}. \tag{61}$$

Similar to the procedure used in previous section, the velocity profile, interfacial velocity, and pressure gradient can be simplified, respectively, as

$$u_f(y) = \frac{\delta^2}{\mu_f}\left(-\frac{dP}{dz}\right)\int_0^{y/\delta}\left(1-\frac{y}{\delta}\right)\left(1+\frac{\varepsilon_m}{\nu_f}\right)^{-1} d\left(\frac{y}{\delta}\right) + \frac{\delta}{\mu_f}\left(\tau_i + \frac{\Gamma_d u_c - \Gamma_{fg} u_i}{\pi D}\right)\int_0^{y/\delta}\left(1+\frac{\varepsilon_m}{\nu_f}\right)^{-1} d\left(\frac{y}{\delta}\right), \tag{62}$$

$$u_i = \frac{\delta\left(-\frac{dP}{dz}\right)\int_0^1\left(1-\frac{y}{\delta}\right)\left(1+\frac{\varepsilon_m}{\nu_f}\right)^{-1} d\left(\frac{y}{\delta}\right) + \left(\tau_i + \frac{\Gamma_d u_c}{P_f}\right)\int_0^1\left(1+\frac{\varepsilon_m}{\nu_f}\right)^{-1} d\left(\frac{y}{\delta}\right)}{\frac{\mu_f}{\delta} + \frac{\Gamma_{fg}}{P_f}\int_0^1\left(1+\frac{\varepsilon_m}{\nu_f}\right)^{-1} d\left(\frac{y}{\delta}\right)} \tag{63}$$

and

$$-\frac{dP}{dz} = \frac{\frac{\mu_f \dot{m}_f}{\rho_f \pi D \delta^2} - \left(\tau_i + \frac{\Gamma_d u_c - \Gamma_{fg} u_i}{\pi D}\right)\int_0^1\left[\int_0^{y/\delta}\left(1+\frac{\varepsilon_m}{\nu_f}\right)^{-1} d\left(\frac{y}{\delta}\right)\right] d\left(\frac{y}{\delta}\right)}{\delta\int_0^1\left[\int_0^{y/\delta}\left(1-\frac{y}{\delta}\right)\left(1+\frac{\varepsilon_m}{\nu_f}\right)^{-1} d\left(\frac{y}{\delta}\right)\right] d\left(\frac{y}{\delta}\right)}. \tag{64}$$

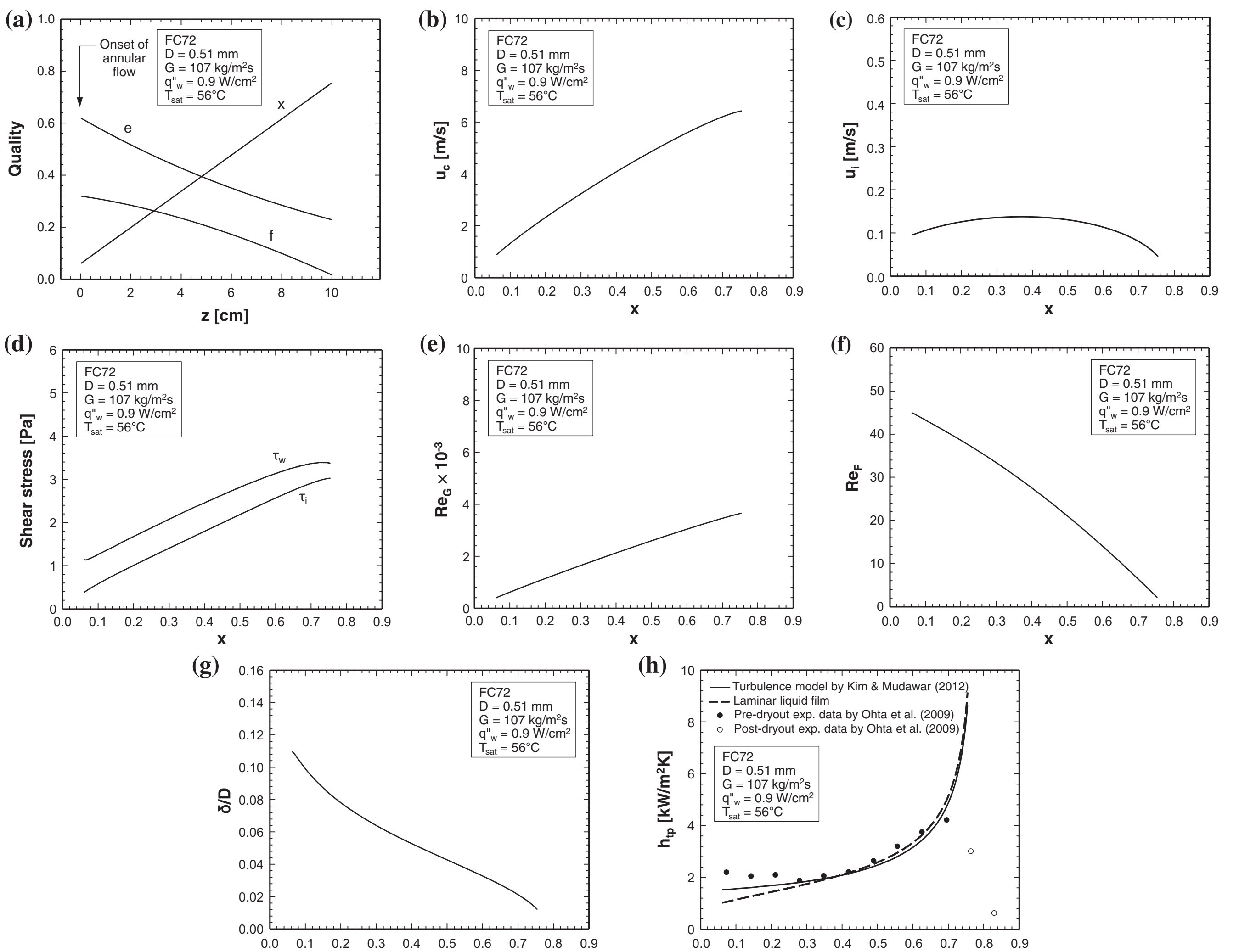


**Fig. 5.** Variations of (a) quality along stream-wise direction, and (b) mean vapor core velocity, (c) interfacial velocity, (d) wall and interfacial shear stresses, (e) vapor core Reynolds number, (f) liquid film Reynolds number, (g) liquid film thickness, and (h) local two-phase heat transfer coefficient with quality for FC72 flow with $D$ = 0.51 mm, $G$ = 107 kg/m$^2$ s, $q''_w$ = 0.9 W/cm$^2$ and $T_{sat}$ = 56 °C corresponding to experimental operating conditions of Ohta et al. [54].

The predictive differences of the average heat transfer coefficient between the complete and simplified models average only 2.0%, with a maximum difference of 2.7%. Although both models yield very close results, all of the subsequent calculations are based on the complete model.

## 3. Model results

Fig. 4(a)–(c) shows model predictions of eddy diffusivity, dimensionless velocity and dimensionless temperature profiles, respectively, of three select cases for different working fluids: FC72, water and R32, corresponding to specific operating conditions of Ohta et al. [54], Bang et al. [55] and Li et al. [57], respectively. The eddy diffusivity profile given by Eq. (50) yields values for dimensionless film thickness, $y^+ = \delta^+$, up to about 18 at the middle of the channel, which is close to the outer edge of the viscous sublayer for typical turbulent flows. The present diffusivity profile is justified by the fact that Van-Driest model is applicable near the solid wall region where $y^+ \leqslant 30$. Due to the interfacial dampening term, $(1 - y^+/\delta^+)^{0.1}$, in the eddy momentum diffusivity profile, $\varepsilon_m/\nu_f$ is reduced to zero at the liquid film interface. The unusual temperature rise in the immediate vicinity of the film interface, which is captured in Fig. 4(c), is caused by the dampening term. Notice that, unlike the cases of water and R32, the eddy momentum diffusivity of FC72 is negligibly small. This suggests that turbulence effects in the FC72 liquid film are insignificant. More details concerning turbulence effects will be discussed below.

Figs. 5–7 show predicted variations of several key parameters for three select cases corresponding to FC72, water and R32, respectively. The liquid film and vapor core Reynolds numbers are defined, respectively, as

$$Re_F = \frac{4\rho_f u_{f,m}\delta}{\mu_f} \tag{65}$$

and

$$Re_G = \frac{\rho_g u_c D_{h,c}}{\mu_g}, \tag{66}$$

where the mean liquid film velocity, $u_{f,m}$, is expressed as

$$u_{f,m} = \frac{\dot{m}_f}{\rho_f (A_{ch} - A_c)} \tag{67}$$

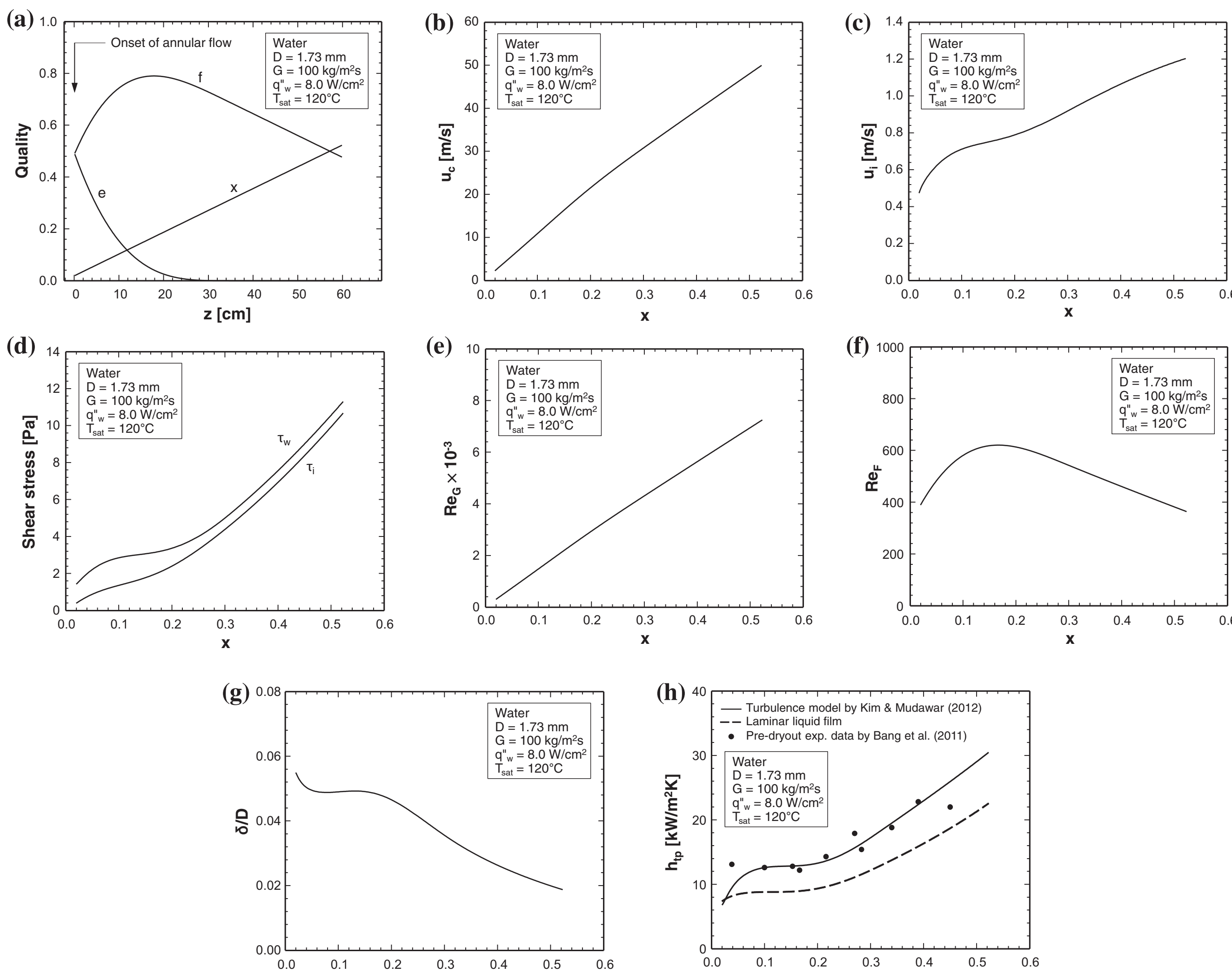


**Fig. 6.** Variations of (a) quality along stream-wise direction, and (b) mean vapor core velocity, (c) interfacial velocity, (d) wall and interfacial shear stresses, (e) vapor core Reynolds number, (f) liquid film Reynolds number, (g) liquid film thickness, and (h) local two-phase heat transfer coefficient with quality for water flow with $D$ = 1.73 mm, $G$ = 100 kg/m$^2$ s, $q''_w$ = 8.0 W/cm$^2$ and $T_{sat}$ = 120 °C corresponding to experimental operating conditions of Bang et al. [55].

and the cross-sectional area of the channel, $A_{ch}$, in Eq. (67) is given by

$$A_{ch} = \frac{\pi}{4} D^2. \tag{68}$$

As liquid is gradually converted to vapor by evaporation, the mean velocity of the vapor core, $u_c$, and the vapor core Reynolds number, $Re_G$, increase with increasing quality, causing increases in the wall shear stress, $\tau_w$, and interfacial shear stress, $\tau_i$. For water, Fig. 6(a), as the liquid droplet quality, $e$, decreases rapidly along the channel, the liquid film quality, $f$, increases quickly at the upstream region until it reach maximum value. Then $e$ is reduced to zero around the middle of the channel, thus no entrained droplets exist in the vapor core farther downstream. Because of gradual evaporation along the channel, the liquid film thickness, $\delta$, decreases with increasing quality at a steeper rate than $f$ does, causing the interfacial velocity, $u_i$, to increase with increasing quality, Fig. 6(c). In contrast, for FC72 and R32, Fig. 5(a) and Fig. 7(a), respectively, the initial liquid droplet quality, $e_0$, is higher than for water, Fig. 6(a), and $e$ decreases at a slower rate. This implies that liquid droplets are entrained in the vapor core over the entire channel length. The liquid film Reynolds number, $Re_F$, $u_i$ and $f$ approach zero where dryout of the liquid film is expected. The heat transfer coefficient increases with increasing quality as the liquid film thins, which eventually leads to film dryout where the heat transfer coefficient begins to decrease sharply. The present annular model accurately captures the experimental heat transfer coefficient data in both magnitude and trend, as shown in Figs. 5(h), 6(h) and 7(h). The model also accurately predicts the location of dryout as depicted in Figs. 5(h) and 7(h).

As discussed in Kim and Mudawar [50], strong interfacial shear can promote turbulent film flow even for relatively small film Reynolds numbers, $Re_F$. To examine the influence of based on the assumption of laminar liquid film. For water and R32, Figs. 6(f) and 7(f), respectively, show the annular model with the turbulent liquid film yields higher heat transfer coefficient values than with the laminar liquid film despite the relatively small $Re_F$ values (smaller than 650 for water and 500 for R32). However, for FC72, both models provide fairly similar heat transfer coefficient results due to the vanishingly small turbulence effects in the FC72 liquid film as shown in Fig. 4(a). Very small $Re_F$ values (smaller than 50), Fig. 5(f), further validate the assumption of laminar liquid film for FC72.

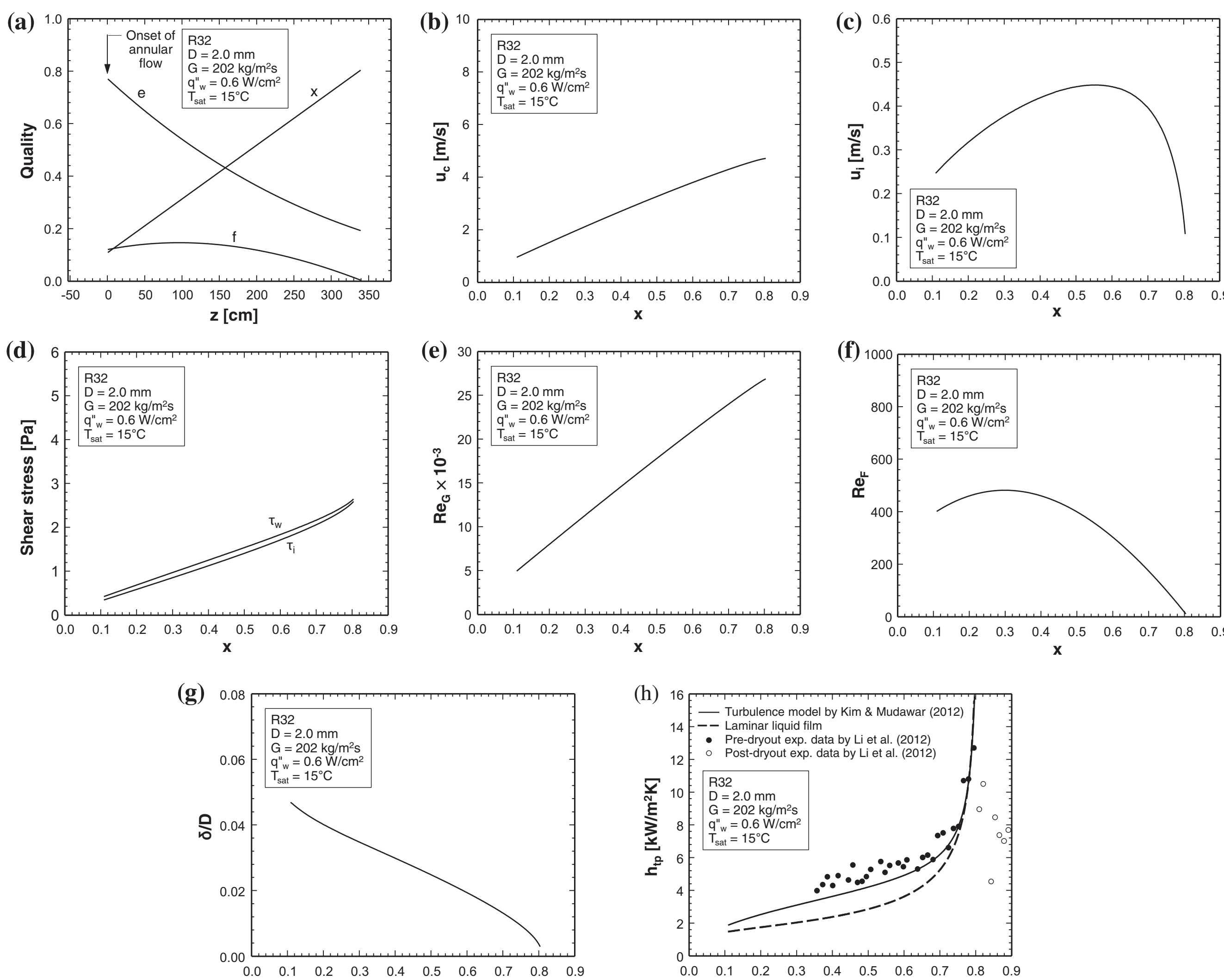


**Fig. 7.** Variations of (a) quality along stream-wise direction, and (b) mean vapor core velocity, (c) interfacial velocity, (d) wall and interfacial shear stresses, (e) vapor core Reynolds number, (f) liquid film Reynolds number, (g) liquid film thickness, and (h) local two-phase heat transfer coefficient with quality for R32 flow with $D$ = 2.0 mm, $G$ = 202 kg/m$^2$ s, $q''_w$ = 0.6 W/cm$^2$ and $T_{sat}$ = 15 °C corresponding to experimental operating conditions of Li et al. [57].

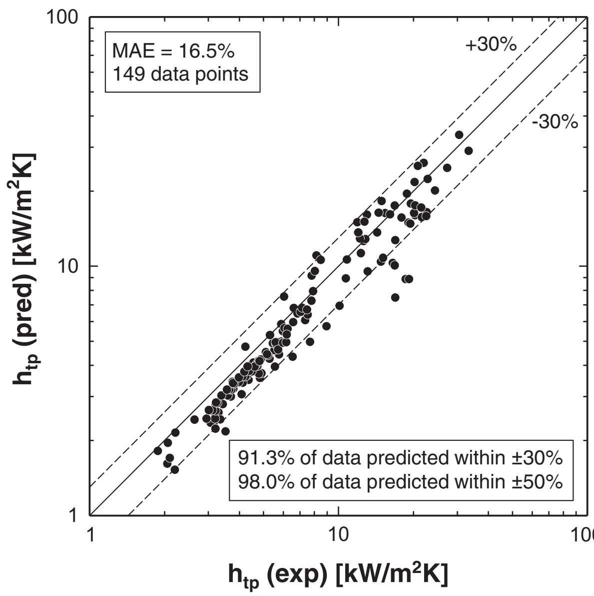


**Fig. 8.** Comparison of predictions of new model with experimental local heat transfer coefficient data for convective boiling dominant saturated flow boiling in circular mini/micro-channels.

Fig. 8 compares predictions of the present model with local convective boiling dominant heat transfer data in circular mini/micro-channels. The mean absolute error (MAE), defined as

$$MAE = \frac{1}{N}\sum \frac{|h_{tp,pred} - h_{tp,exp}|}{h_{tp,exp}} \times 100\%, \tag{69}$$

is used to assess the predictive accuracy of the model. The model shows excellent accuracy against the 149 convective boiling dominant data points from Table 1, with a MAE of 16.5%, and 91.3% and 98.0% of the data falling within ±30% and ±50% error bands, respectively. Table 1 shows the present model also predicts individual databases with good accuracy.

Further improvement to the accuracy of this model is possible with future experimental studies to better predict entrainment and deposition effects in small channels. Improvements are also possible by measuring eddy diffusivity profile in shear driven films. Because of the small liquid thickness in these flows, useful information on turbulence in films can be realized from studies of wavy, free-falling films [71,72], and use of advanced diagnostic tools to measure instantaneous film thickness [73–76], velocity profile [75,76] and temperature profile [73,74] across the film.

## 4. Conclusions

This study examined two-phase heat transfer characteristics associated with annular flow boiling in circular mini/micro-channels subjected to a uniform circumferential heat flux. A theoretical control-volume-based model was developed based on the assumptions of smooth interface between the annular liquid film and vapor core, and circumferential uniformity of film thickness. The model's predictive accuracy was assessed against 149 data points of local two-phase heat transfer coefficient associated with convective boiling dominant heat transfer for saturated flow boiling in circular mini/micro-channels. Key conclusions from the study are as follows.

(1) The control-volume-based method is very effective at incorporating the complex mass, momentum and heat transfer characteristics in annular flow.
(2) Droplet entrainment and deposition effects are accurately accounted for in the model using new correlations for initial liquid droplet quality at the onset of annular flow, and deposition mass transfer coefficient, respectively.
(3) For shear-driven films, transition from laminar to turbulent film flow may occur at unusually small film Reynolds numbers. Turbulent effects must therefore be accounted for when modeling the transport behavior of the annular film.
(4) Interfacial dampening of turbulent eddies is accurately accounted for in the model with the aid of an eddy diffusivity model specifically tailored to turbulent shear-driven films.
(5) The new model accurately predicts local heat transfer coefficient data for the convective boiling dominant regime, evidenced by an overall mean absolute error of 16.5%, with 91.3% and 98.0% of the data falling within ±30% and ±50% error bands, respectively.

## Acknowledgement

The authors are grateful for the partial support for this project from the National Aeronautics and Space Administration (NASA) under Grant No. NNX13AC83G.

## References

[1] T.C. Willingham, I. Mudawar, Forced-convection boiling and critical heat flux from a linear array of discrete heat sources, Int. J. Heat Mass Transfer 35 (1992) 2879–2890.
[2] T.N. Tran, M.W. Wambsganss, D.M. France, Small circular- and rectangular-channel boiling with two refrigerants, Int. J. Multiphase Flow 22 (1996) 485–498.
[3] H.J. Lee, S.Y. Lee, Heat transfer correlation for boiling flows in small rectangular horizontal channels with low aspect ratios, Int. J. Multiphase Flow 27 (2001) 2043–2062.
[4] L.-T. Yeh, R.C. Chu, Thermal Management of Microelectronic Equipment: Heat Transfer Theory, Analysis Methods, and Design Practices, ASME, New York, 2002.
[5] S. Mukherjee, I. Mudawar, Smart pumpless loop for micro-channel electronic cooling using flat and enhanced surfaces, IEEE Trans. Compon. Packag. Technol. 26 (2003) 99–109.
[6] S. Mukherjee, I. Mudawar, Pumpless loop for narrow channel and micro-channel boiling from vertical surfaces, J. Electron. Packag. Trans. ASME 125 (2003) 431–441.
[7] S.M. Kim, J. Kim, I. Mudawar, Flow condensation in parallel rectangular micro-channels – part 1: experimental results and assessment of pressure drop correlations, Int. J. Heat Mass Transfer 55 (2012) 971–983.
[8] S.M. Kim, I. Mudawar, Flow condensation in parallel rectangular micro-channels – part 2: heat transfer results and correlation technique, Int. J. Heat Mass Transfer 55 (2012) 984–994.
[9] T.M. Anderson, I. Mudawar, Microelectronic cooling by enhanced pool boiling of a dielectric fluorocarbon liquid, J. Heat Transfer Trans. ASME 111 (1989) 752–759.
[10] I. Mudawar, A.H. Howard, C.O. Gersey, An analytical model for near-saturated pool boiling CHF on vertical surfaces, Int. J. Heat Mass Transfer 40 (1997) 2327–2339.
[11] A.H. Howard, I. Mudawar, Orientation effects on pool boiling CHF and modeling of CHF for near-vertical surfaces, Int. J. Heat Mass Transfer 42 (1999) 1665–1688.
[12] Y. Katto, M. Kunihiro, Study of the mechanism of burn-out in boiling system of high burn-out heat flux, Bull. JSME 16 (1973) 1357–1366.
[13] M. Monde, T. Inoue, Critical heat flux in saturated forced convective boiling on a heated disk with multiple impinging jets, J. Heat Transfer Trans. ASME 113 (1991) 722–727.
[14] D.C. Wadsworth, I. Mudawar, Enhancement of single-phase heat transfer and critical heat flux from an ultra-high-flux-source to a rectangular impinging jet of dielectric liquid, J. Heat Transfer Trans. ASME 114 (1992) 764–768.
[15] M.E. Johns, I. Mudawar, An ultra-high power two-phase jet-impingement avionic clamshell module, J. Electron. Packag. Trans. ASME 118 (1996) 264–270.
[16] S. Toda, A study in mist cooling (1st report: investigation of mist cooling), Trans. JSME 38 (1972) 581–588.
[17] L. Lin, R. Ponnappan, Heat transfer characteristics of spray cooling in a closed loop, Int. J. Heat Mass Transfer 46 (2003) 3737–3746.
[18] J.R. Rybicki, I. Mudawar, Single-phase and two-phase cooling characteristics of upward-facing and downward-facing sprays, Int. J. Heat Mass Transfer 49 (2006) 5–16.

[19] M. Visaria, I. Mudawar, Theoretical and experimental study of the effects of spray orientation on two-phase spray cooling and critical heat flux, Int. J. Heat Mass Transfer 51 (2008) 2398–2410.
[20] W. Nakayama, T. Nakajima, S. Hirasawa, Heat sink studs having enhanced boiling surfaces for cooling of microelectronic components, ASME Paper 84-WA/HT-89, 1984.
[21] R.L. Webb, The evolution of enhanced surface geometries for nucleate boiling, Heat Transfer Eng. 2 (1981) 46–69.
[22] V. Khanikar, I. Mudawar, T. Fisher, Effects of carbon nanotube coating on flow boiling in a micro-channel, Int. J. Heat Mass Transfer 52 (2009) 3805–3817.
[23] M.K. Sung, I. Mudawar, Single-phase hybrid micro-channel/jet impingement cooling, Int. J. Heat Mass Transfer 51 (2008) 4342–4352.
[24] M.K. Sung, I. Mudawar, Single-phase and two-phase heat transfer characteristics of low temperature hybrid micro-channel/micro-jet impingement cooling module, Int. J. Heat Mass Transfer 51 (2008) 3882–3895.
[25] R.W. Lockhart, R.C. Martinelli, Proposed correlation of data for isothermal two-phase, two-component flow in pipes, Chem. Eng. Prog. 45 (1949) 39–48.
[26] D.S. Jung, R. Radermacher, Prediction of pressure drop during horizontal annular flow boiling of pure and mixed refrigerants, Int. J. Heat Mass Transfer 32 (1989) 2435–2446.
[27] C.C. Wang, C.S. Chiang, D.C. Lu, Visual observation of two-phase flow pattern of R-22, R-134a, and R-407C in a 6.5-mm smooth tube, Exp. Therm. Fluid Sci. 15 (1997) 395–405.
[28] K. Mishima, T. Hibiki, Some characteristics of air–water two-phase flow in small diameter vertical tubes, Int. J. Multiphase Flow 22 (1996) 703–712.
[29] H.J. Lee, S.Y. Lee, Pressure drop correlations for two-phase flow within horizontal rectangular channels with small heights, Int. J. Multiphase Flow 27 (2001) 783–796.
[30] W. Li, Z. Wu, A general correlation for adiabatic two-phase pressure drop in micro/mini-channels, Int. J. Heat Mass Transfer 53 (2010) 2732–2739.
[31] G.M. Lazarek, S.H. Black, Evaporative heat transfer, pressure drop and critical heat flux in a small vertical tube with R-113, Int. J. Heat Mass Transfer 25 (1982) 945–960.
[32] M.M. Shah, Chart correlation for saturated boiling heat transfer: equations and further study, ASHRAE Trans. 88 (1982) 185–196.
[33] W. Yu, D.M. France, M.W. Wambsganss, J.R. Hull, Two-phase pressure drop, boiling heat transfer, and critical heat flux to water in a small-diameter horizontal tube, Int. J. Multiphase Flow 28 (2002) 927–941.
[34] W. Li, Z. Wu, A general correlation for evaporative heat transfer in micro/mini-channels, Int. J. Heat Mass Transfer 53 (2010) 1778–1787.
[35] S.M. Kim, I. Mudawar, Universal approach to predicting two-phase frictional pressure drop for adiabatic and condensing mini/micro-channel flows, Int. J. Heat Mass Transfer 55 (2012) 3246–3261.
[36] S.M. Kim, I. Mudawar, Universal approach to predicting two-phase frictional pressure drop for mini/micro-channel saturated flow boiling, Int. J. Heat Mass Transfer 58 (2013) 718–734.
[37] S.M. Kim, I. Mudawar, Universal approach to predicting heat transfer coefficient for condensing mini/micro-channel flows, Int. J. Heat Mass Transfer 56 (2013) 238–250.
[38] S.M. Kim, I. Mudawar, Universal approach to predicting saturated flow boiling heat transfer in mini/micro-channels – part II. Two-phase heat transfer coefficient, Int. J. Heat Mass Transfer 64 (2013) 1239–1256.
[39] S.M. Kim, I. Mudawar, Universal approach to predicting saturated flow boiling heat transfer in mini/micro-channels – part I. Dryout incipience quality, Int. J. Heat Mass Transfer 64 (2013) 1226–1238.
[40] D.D. Hall, I. Mudawar, Ultra-high critical heat flux (CHF) for subcooled water flow boiling – II. High-CHF database and design parameters, Int. J. Heat Mass Transfer 42 (1999) 1429–1456.
[41] D.D. Hall, I. Mudawar, Critical heat flux (CHF) for water flow in tubes – I. Compilation and assessment of world CHF data, Int. J. Heat Mass Transfer 43 (2000) 2573–2604.
[42] D.D. Hall, I. Mudawar, Critical heat flux (CHF) for water flow in tubes – II. Subcooled CHF correlations, Int. J. Heat Mass Transfer 43 (2000) 2605–2640.
[43] C.O. Cersey, I. Mudawar, Effects of heater length and orientation on the trigger mechanism for near-saturated flow boiling critical heat flux – I. Photographic study and statistical characterization of the near-wall interfacial features, Int. J. Heat Mass Transfer 38 (1995) 629–641.
[44] C.O. Cersey, I. Mudawar, Effects of heater length and orientation on the trigger mechanism for near-saturated flow boiling critical heat flux – II. Critical heat flux model, Int. J. Heat Mass Transfer 38 (1995) 643–654.
[45] J.C. Sturgis, I. Mudawar, Critical heat flux in a long, rectangular channel subjected to onesided heating – I. Flow visualization, Int. J. Heat Mass Transfer 42 (1999) 1835–1847.
[46] J.C. Sturgis, I. Mudawar, Critical heat flux in a long, rectangular channel subjected to onesided heating – II. Analysis of critical heat flux data, Int. J. Heat Mass Transfer 42 (1999) 1849–1862.
[47] H. Zhang, I. Mudawar, M.M. Hasan, Experimental assessment of the effects of body force, surface tension force, and inertia on flow boiling CHF, Int. J. Heat Mass Transfer 45 (2002) 4079–4095.
[48] H. Zhang, I. Mudawar, M.M. Hasan, Flow boiling CHF in microgravity, Int. J. Heat Mass Transfer 48 (2005) 3107–3118.
[49] J. Lee, I. Mudawar, Experimental investigation and theoretical model for subcooled flow boiling pressure drop in microchannel heat sinks, J. Electron. Packag. Trans. ASME 131 (2009) 031008.
[50] S.M. Kim, I. Mudawar, Theoretical model for annular flow condensation in rectangular micro-channels, Int. J. Heat Mass Transfer 55 (2012) 958–970.
[51] W. Qu, I. Mudawar, Transport phenomena in two-phase micro-channel heat sinks, J. Electron. Packag. Trans. ASME 126 (2004) 213–224.
[52] B. Sumith, F. Kaminaga, K. Matsumura, Saturated flow boiling of water in a vertical small diameter tube, Exp. Therm. Fluid Sci. 27 (2003) 789–801.
[53] S. Saitoh, H. Daiguji, E. Hihara, Effect of tube diameter on boiling heat transfer of R-134a in horizontal small-diameter tubes, Int. J. Heat Mass Transfer 48 (2005) 4973–4984.
[54] H. Ohta, K. Inoue, M. Ando, K. Watanabe, Experimental investigation on observed scattering in heat transfer characteristics for flow boiling in a small diameter tube, Heat Transfer Eng. 30 (2009) 19–27.
[55] K.H. Bang, K.K. Kim, S.K. Lee, B.W. Lee, Pressure effect on flow boiling heat transfer of water in minichannels, Int. J. Therm. Sci. 50 (2011) 280–286.
[56] H.K. Oh, C.H. Son, Evaporation flow pattern and heat transfer of R-22 and R-134a in small diameter tubes, Heat Mass Transfer 47 (2011) 703–717.
[57] M. Li, C. Dang, E. Hihara, Flow boiling heat transfer of HFO1234yf and R32 refrigerant mixtures in a smooth horizontal tube: part I. Experimental investigation, Int. J. Heat Mass Transfer 55 (2012) 3437–3446.
[58] W. Qu, I. Mudawar, Flow boiling heat transfer in two-phase micro-channel heat sinks-II. Annular two-phase flow model, Int. J. Heat Mass Transfer 46 (2003) 2773–2784.
[59] Y. Taitel, A.E. Dukler, A model for predicting flow regime transitions in horizontal and near horizontal gas-liquid flow, AIChE J. 22 (1976) 47–55.
[60] P.B. Whalley, P. Hutchinson, G.F. Hewitt, The calculation of critical heat flux in forced convection boiling, in: Proc. Fifth Int. Heat Transfer Conf., Tokyo, Japan, Paper B6.11, 1974, pp. 290–294.
[61] I.I. Paleev, B.S. Filippovich, Phenomena of liquid transfer in two-phase dispersed annular flow, Int. J. Heat Mass Transfer 9 (1966) 1089–1093.
[62] G.F. Hewitt, A.H. Govan, Phenomenological modeling of non-equilibrium flows with phase change, Int. J. Heat Mass Transfer 33 (1990) 229–242.
[63] S. Sugawara, Droplet deposition and entrainment modeling based on the three-fluid model, Nucl. Eng. Des. 122 (1990) 67–84.
[64] G.B. Wallis, One Dimensional Two-phase Flow, McGraw-Hill, New York, 1969.
[65] R.K. Shah, A.L. London, Laminar Flow Forced Convection in Ducts: A Source Book for Compact Heat Exchanger Analytical Data, Supl. 1, Academic press, New York, 1978.
[66] E.R. Van Driest, On turbulent flow near a wall, J. Aeronaut. Sci. 23 (1956) 1007–1011.
[67] W.M. Kays, Heat transfer to the transpired turbulent boundary layer, Int. J. Heat Mass Transfer 15 (1972) 1023–1044.
[68] W.M. Kays, M.E. Crawford, Convective Heat and Mass Transfer, second ed., McGraw-Hill, New York, 1980.
[69] I. Mudawar, M.A. El-Masri, Momentum and heat transfer across freely-falling turbulent liquid films, Int. J. Multiphase flow 12 (1986) 771–790.
[70] H. Ueda, R. Moller, S. Komori, T. Mizushima, Eddy diffusivity near the free surface of open channel flow, Int. J. Heat Mass Transfer 20 (1977) 1127–1136.
[71] J.A. Shmerler, I. Mudawar, Local heat transfer coefficient in wavy free-falling turbulent liquid films undergoing uniform sensible heating, Int. J. Heat Mass Transfer 31 (1988) 67–77.
[72] J.A. Shmerler, I. Mudawar, Local evaporative heat transfer coefficient in turbulent free-falling liquid films, Int. J. Heat Mass Transfer 31 (1988) 731–742.
[73] T.H. Lyu, I. Mudawar, Statistical investigation of the relationship between interfacial waviness and sensible heat transfer to a falling liquid film, Int. J. Heat Mass Transfer 34 (1991) 1451–1464.
[74] T.H. Lyu, I. Mudawar, Determination of wave-induced fluctuations of wall temperature and convective heat transfer coefficient in the heating of a turbulent falling liquid film, Int. J. Heat Mass Transfer 34 (1991) 2521–2534.
[75] I. Mudawar, R.A. Houpt, Mass and momentum transport in falling liquid films laminarized at relatively high Reynolds numbers, Int. J. Heat Mass Transfer 36 (1993) 3437–3448.
[76] I. Mudawar, R.A. Houpt, Measurement of mass and momentum transport in wavy-laminar falling liquid films, Int. J. Heat Mass Transfer 36 (1993) 4151–4162.